Retinal Pathology in a Canine Model of Late Infantile Neuronal Ceroid Lipofuscinosis

Martin L. Katz,[1,2] *Joan R. Coates,*[3] *Jocelyn J. Cooper,*[3,4] *Dennis P. O'Brien,*[3] *Manbok Jeong,*[3,5,6] *and Kristina Narfström*[1,3]

Purpose. Late infantile neuronal ceroid lipofuscinosis (NCL) is an inherited disorder characterized by progressive vision loss. The disease results from mutations in the *TPP1* (*CLN2*) gene. Studies were undertaken to characterize the effects of a *TPP1* frameshift mutation on the retina in Dachshunds.

Methods. A litter of four puppies consisting of one homozygous affected dog, two heterozygotes, and one homozygous normal dog were monitored for neurologic and retinal changes through 10 months of age. The affected and homozygous normal dogs, as well as one of the heterozygotes, were then euthanatized, and the retinas were examined morphologically.

Results. The affected dog exhibited normal visual behavior and retinal function at 3 months of age, but vision was clearly impaired by 7 months, with markedly reduced ERG b-wave amplitudes. Beyond 7 months of age, the affected dog was functionally blind, and pupillary light reflexes and ERG response amplitudes continued to decline through 10 months of age. Both rod and cone system functions were severely impaired. The retina exhibited accumulation of autofluorescent storage bodies with distinctive curvilinear contents. Substantial cell loss occurred in the inner nuclear layer, with a smaller reduction in photoreceptor cell density.

Conclusions. The canine *TPP1* mutation results in progressive vision loss and retinal degeneration similar to that which occurs in human late infantile NCL. With the canine model, the natural history of disease progression in the retina provides a better understanding of the pathologic course of the disease and provides objective markers that can be used to assess the efficacy of therapeutic interventions. (*Invest Ophthalmol Vis Sci.* 2008;49:2686–2695) DOI:10.1167/iovs.08-1712

From the [1]Mason Eye Institute, University of Missouri School of Medicine, the Departments of [2]Veterinary Pathobiology and [3]Medicine and Surgery, University of Missouri, College of Veterinary Medicine, Columbia, Missouri; and the [5]Department of Veterinary Surgery and Ophthalmology, College of Veterinary Medicine, and [6]BK21 Program for Veterinary Science, Seoul National University, Seoul, Republic of Korea.

[4]Present affiliation: Department of Small Animal Clinical Sciences, College of Veterinary Medicine and Biomedical Sciences, Texas A&M University, College Station, Texas.

Supported by an unrestricted grant from Research to Prevent Blindness to the Mason Eye Institute and by grants from the University of Missouri Research Board and the Batten Disease Support and Research Association, with partial matching support from the University of Missouri PRIME (Program for Research Infrastructure and Matching Expenses) fund.

Submitted for publication January 9, 2008; revised February 19, 2008; accepted April 24, 2008.

Disclosure: **M.L. Katz**, None; **J.R. Coates**, None; **J.J. Cooper**, None; **D.P. O'Brien**, None; **M. Jeong**, None; **K. Narfström**, None

The publication costs of this article were defrayed in part by page charge payment. This article must therefore be marked "*advertisement*" in accordance with 18 U.S.C. §1734 solely to indicate this fact.

Corresponding author: Martin L. Katz, Mason Eye Institute, University of Missouri School of Medicine, One Hospital Drive, Columbia, MO 65212; katzm@health.missouri.edu.

Childhood-onset neuronal ceroid lipofuscinoses (NCLs) are autosomal recessively inherited lysosomal storage disorders characterized by progressive vision loss culminating in blindness, cognitive and motor decline, and seizures. The NCLs are uniformly fatal. Clinical signs of NCL result from widespread progressive neurodegeneration that is accompanied by intracellular accumulation of autofluorescent storage bodies in nervous and other tissues, including the retina.[1,2] There are several forms of NCL that differ from one another in the age at which symptoms first appear, the rate of disease progression, and the patterns of symptoms.[1,3–5] To date, mutations in eight different genes (*PPT1*, *CLN2*, *CLN3*, *CLN5*, *CLN6*, *CLN8*, *CTSD*, and *MFSD8*) have been found to underlie different forms of NCL.[3,6–8] In almost all patients with NCL, severe vision loss is accompanied by progressive retinal degeneration (Hainsworth DP, Liu G, Hamm CW, Katz ML, manuscript submitted, 2008).[2,9–12] Currently, there are no known treatments to delay or halt the progression of the NCLs, but several approaches to therapy, including gene and stem cell therapies, are under investigation.[13,14]

Development of effective therapeutic interventions will be greatly enhanced with the availability of suitable animal models. Mouse models are available for most of the NCLs, but these models are of limited utility because of the small size, relatively primitive nervous system, and short lifespan of the mouse. In some cases, NCL gene mutations in mice result in only modest phenotypic signs of neurodegeneration.[15] Naturally occurring NCLs have been identified in several larger animal species, including dogs.[16–21] Among the canine NCLs is a form of the disease in Dachshunds that results from a mutation in *TPP1* that encodes the lysosomal enzyme tripeptidyl peptidase 1.[22] Human subjects with mutations in *TPP1* (*CLN2*) have a late infantile form of NCL. Studies were undertaken to characterize the effects of the *TPP1* mutation on the canine retina.

Methods

Animals

A male and a female Dachshund, each of which were heterozygous for a frame shift mutation in the *TPP1* gene,[22] were mated naturally. A litter of four puppies was produced that included one homozygous normal female, two heterozygous males, and one male homozygous for the *TPP1* frame shift mutation. The dogs were housed in a research kennel, were socialized daily, and were taught basic behavioral commands (sit, stay, and down). All studies involving dogs were performed in compliance with the ARVO Statement for the Use of Animals in Ophthalmic and Vision Research and were approved by the University of Missouri Animal Care and Use Committee.

Physical and Neurologic Examinations

Weekly physical and neurologic examinations were performed on all littermates. Genotyping indicated that one puppy was homozygous for the mutant allele ($TPP1^{-/-}$; dog 1), two were heterozygous ($TPP1^{+/-}$; dogs 2 and 3), and one was normal homozygous ($TPP1^{+/+}$; dog 4). Investigators evaluating the dogs were masked to the genotype. Neurologic dysfunction was assessed subjectively by standard clinical neu-

Investigative Ophthalmology & Visual Science, June 2008, Vol. 49, No. 6

rologic examination.[23] Components of the neurologic examination included observation (mentation, posture, and gait), cranial nerve evaluation, postural reaction testing (conscious proprioceptive positioning, hopping, wheelbarrow, tactile placement, and extensor postural thrust), spinal reflexes (myotatic and flexor withdrawal), and nociception (superficial and deep). Gait evaluation was assessed as normal, ataxic, and paretic (ambulatory or nonambulatory). Postural reactions, spinal reflexes, and nociception were assessed as normal, decreased, or absent. Dogs were also evaluated for abnormal movement or seizure activity.

Ophthalmic Examination

Specific ophthalmic evaluation was performed 2 to 4 hours before each electroretinography session when the dogs were 3 months (four littermates), 7 months (four littermates), 8 months (four littermates), and 10 months old (two littermates; dogs 1 and 4). Visual behavior was tested using randomly falling cotton balls, approximately 20 cm in front of each eye in the dark and then in the light, followed by menace responses and pupillary light reflexes (PLRs) in both lighting conditions, the latter using a Finnoff transilluminator (Welch Allyn Distributors; Skaneateles Falls, NY). Pupils were thereafter dilated with a short-acting mydriatic (tropicamide 1%; Alcon, Fort Worth, TX), and indirect ophthalmoscopy (Welch Allyn Distributors) was performed, followed by slit lamp biomicroscopy (SL14; Kowa Co. Ltd., Tokyo, Japan). Fundus appearances were documented with a digital fundus camera (NM-100; Nidek Co. Ltd., Freemont, CA) at least 1 week after each specific ophthalmic procedure (including electroretinography; ERG).

Electroretinography

Unilateral ERG evaluations were performed with a portable ERG unit (HMsERG model 1000; RetVet Corp., Columbia, MO), with the mini-Ganzfeld dome positioned approximately 1 cm from the right tested eye. The dogs were deeply sedated by using medetomidine (Domitor; Novartis, Pfizer Animal Health, Exton, PA), up to 46 μg/10 kg, equivalent to 0.45 mL/10 kg, and prepared for the ERG session in ordinary room light. Heart and respiratory rates were closely monitored throughout the procedure, and the dogs were temperature controlled. The dog's head was positioned on a deflatable cushion to ensure complete stability. Maximum pupillary dilatation was provided for by the use of a short-acting mydriatic and was further topically anesthetized (Alcaine; Alcon). A lid speculum was inserted to ensure that the nictitating membrane and the upper and lower eyelids did not interfere with light exposure of the maximally dilated pupils. Platinum subdermal needle electrodes (Model E2; Grass Instrument Division, Astro-Med, Inc., West Warwick, RI) were used for the ground electrode, positioned on the occipital crest, and for the reference electrode, positioned 3 to 4 cm (depending on the dog's age) from the lateral canthus, close to the base of the right ear. An active contact lens electrode (ERG-Jet; Universo Plastique, LKC Technologies Inc., Gaithersburg, MD) was placed on the cornea after instillation of one drop of 2% methylcellulose (Methocel; Ciba Vision, Munich, Germany). The electrodes were connected to a preamplifier, and the signals were amplified with a band-pass filter between 0.3 and 300 Hz.

Each ERG session consisted of scotopic and photopic ERGs in accordance with the Dog Diagnostic Protocol, recommended by the European College of Veterinary Ophthalmology, primarily for evaluation of rod and cone function.[24] This protocol is preprogramed on the ERG unit and is executed automatically on initiation of the ERG session by the examiner (Jeong M, Narfstrom K, Son W, et al., manuscript submitted, 2008). During 20 minutes of dark adaptation, scotopic low-intensity rod responses were elicited every 4 minutes at a stimulus intensity of 0.01 cd-s/m^2; averaged responses to 10 flashes, given at 2-second intervals, were recorded for each time point. The light stimulus intensity was then increased to 3 cd-s/m^2 and the averaged responses to four flashes at 10-second intervals were recorded. Thereafter, scotopic high-intensity responses were elicited using 10 cd-s/m^2; averaged responses to four flashes administered at 20-second intervals were recorded. The latter two recordings depicted responses from both rods and cones. After 10 minutes of light adaptation with a background luminance of 30 cd/m^2, photopic single-flash responses were recorded using 3 cd-s/m^2 of flash stimulus, averaging 32 flashes at an interval of 0.5 seconds, followed by evaluation of 30-Hz photopic flicker at the same light intensity stimulation. The latter two recordings were performed to evaluate cone and inner retina function, respectively. Data were collected automatically on the compact flash card of the ERG unit, transferred to a computer, printed, and stored for further analysis. ERG curve forms in all recordings were evaluated, and the amplitudes and implicit times for the a- and b-waves were measured as previously described.[25]

After termination of the ERG session an injection of atipamezole (Antisedan; Pfizer Inc. St Louis, MO) was administered intramuscularly to reverse the deep sedation (at a dosage five times higher than that given of the medetomidine, i.e., similar volumes were injected).

Morphologic Analyses

Three of the littermates, a normal female (dog 4), a carrier male (dog 2), and a homozygous affected male (dog 1), were euthanatized at 10.5 months of age by intravenous infusion (Beuthanasia-D-Special; Schering Plough Animal Health, Omaha, NE). The eyes of each dog were enucleated immediately after death. The anterior portions of the eyes, including the cornea, iris, lens, and vitreous, were removed, and the remainder of each eye was placed in a fixative solution. One eye of each dog was fixed in electron microscopy (EM) fixative (2.0% glutaraldehyde, 1.12% paraformaldehyde, 0.13 M sodium cacodylate, and 0.13 mM $CaCl_2$; pH 7.40) and the other eye was fixed in fluorescence microscopy (FM) fixative (0.1% glutaraldehyde, 3.5% paraformaldehyde, 0.13 M sodium cacodylate, and 0.13 mM $CaCl_2$; pH 7.40). After 1 hour of incubation with gentle agitation in FM fixative at room temperature, the samples to be used for fluorescence microscopic analysis were incubated in 0.17 M sodium cacodylate with gentle agitation for at least 1 hour. The eyecups were then dissected to obtain selected areas from the inferior and superior central regions of the retina (Fig. 1). These samples were embedded (Tissue-Tek; Sakura Finetek, Torrance, CA) and frozen on dry ice. Eyecups that had been placed in EM fixative were incubated with gentle agitation for at least

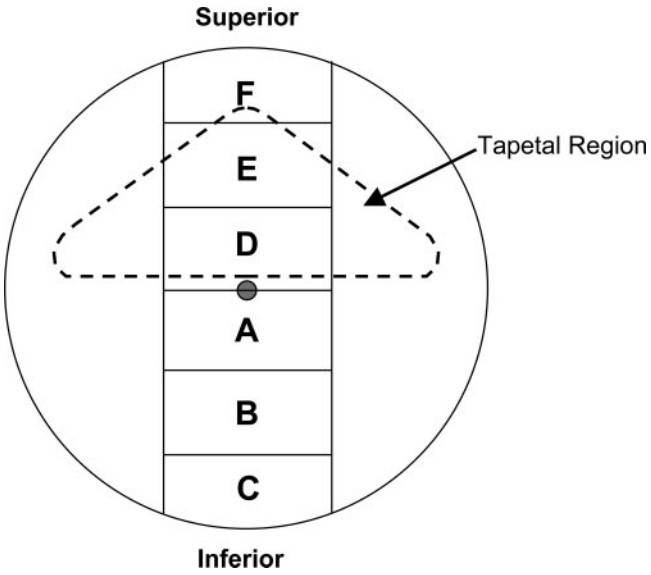

Figure 1. Diagram illustrating how the eyes used for morphologic analyses were dissected. After removal of the anterior portions of the eye up to the ora serrata, the eyecup was dissected to obtain six regions (A–F). Sections were cut from the regions indicated by the lines separating regions A and B (nontapetal) and D and E (tapetal). *Dashed line*: approximate extent of the tapetal area of the dog fundus.

2 hours at room temperature. The eyecups were then dissected to obtain the same regions as those obtained for fluorescence microscopy from the fellow eye of the same dog (Fig. 1). Samples from these regions were postfixed in 1% osmium tetroxide and embedded in epoxy resin.

Five-micrometer-thick sections were cut from the Tissue-Tek–embedded samples and mounted on glass slides (Super Frost; Fisher Scientific, Pittsburgh, PA) in 0.17 M sodium cacodylate. The sections were examined with a microscope (Axiophot; Carl Zeiss Meditec, Inc., Dublin, CA) equipped with epi-illumination from a high-pressure, 50-W mercury vapor lamp, a 40× objective lens (Plan-Neofluar) with a 1.3 numerical aperture, a 395- to 440-nm band-pass exciter filter, and chromatic beam splitter (FT 460), and an barrier filter (LP 515; all from Carl Zeiss Meditec, Inc.). Photography was performed with daylight-balanced, color-positive film (Elite-Chrome 100; Eastman-Kodak, Rochester, NY).

For ultrastructural and light microscopic (LM) morphologic analyses, the selected portions of the eyes that had been fixed with EM fixative were washed with 0.17 M sodium cacodylate (pH 7.4) followed by secondary fixation in 1% osmium tetroxide. Subsequently, the samples were dehydrated via sequential incubation in increasing concentrations of acetone and embedded in epoxy resin. Sections of the embedded samples were cut for both LM and EM examinations. For LM, 1-μm-thick sections were mounted on glass slides and were stained with toluidine blue. For EM, sections were mounted on copper grids and were stained with uranyl acetate and lead citrate. Light microscopy (Axiophot; Carl Zeiss Meditec, Inc.) and electron microscopy (model 1200 EX transmission electron microscope; JEOL, Tokyo, Japan) were performed. Cell densities in the inner (INL) and outer nuclear layers (ONL) of the retinas were determined from the toluidine-blue–stained sections. The sections were obtained from the borders between areas A and B and between areas D and E (Fig. 1). Micrographs of each section were obtained that each represented 150 μm of retinal length (as measured along the retinal pigment epithelium; RPE). The numbers of nuclei per 150 μm retinal length were determined for at least six regions of each retina section. Cell density determinations were performed in a masked fashion by a single observer and were performed with the assistance of a computer program (Metamorph; Molecular Devices, Sunnyvale, CA).

Results

Physical and Neurologic Examination Findings

Physical examination findings remained normal for all pups. Neurologic examination in the affected dog revealed dull mentation and cerebellar ataxia beginning at 6.5 months of age. Although mentation was alert up to that point, the affected pup also exhibited prior loss of focus during training for basic behavior commands. Intention tremors developed by 8 months. The ataxia exhibited by the affected dog progressed with age and was considered worse in the pelvic limbs. After the Hallpike maneuver, wide head excursions were elicited by 7.5 months. Asymmetric proprioceptive deficits were evident by 7.5 months of age and worse in the pelvic limbs. Tactile placing of the thoracic limbs was absent by 8 months of age. Postural reaction deficits became symmetric in all limbs by 10 months of age. Spinal reflexes remained intact. Ocular motor abnormalities included decreased physiologic nystagmus and positional downbeat nystagmus by 9 months. At 8 months, the dog startled easily with loud claps. During an ERG procedure at 8 months, with the dog sedated with medetomidine, the affected dog manifested myoclonic jerks. An electroencephalogram/electromyelogram (EEG/EMG) revealed paroxysmal bursts of 7-Hz spike and wave, and spindling in all leads. The myoclonic activity was abolished after IV administration of diazepam (Carpuject; Hospira, Inc., Lake Forest, IL). The myoclonic jerks became spontaneous by 10.5 months. In summary, abnormal neurologic findings included altered mentation and cognitive function, cerebellar ataxia, blindness, and myoclonus. None of these abnormalities was observed in the littermates that were heterozygous or homozygous for the normal *TPP1* allele.

Ophthalmic Examinations

At age 3 months, all puppies showed normal visual behavior, normal menace responses, and pupillary light reflexes. The anterior and posterior segments of the eyes were normal in all littermates on funduscopic and biomicroscopic examination. No abnormalities were found in three of the four littermates throughout the study period. At age 7 months, however, dog 1 showed clearly reduced visual capacity. The menace response was absent from this time point on. In addition, pupillary light reflexes in the dog were incomplete at this age and became markedly sluggish a few weeks later. The dog was considered blind by age 8 months. By 10 months, resting mydriasis was noted in both eyes. Figure 2A shows the bilateral funduscopic changes that were observed in the affected dog; a marked increase in granularity was noted in the midperipheral and peripheral tapetal fundus, and there was generalized vascular attenuation. No apparent funduscopic changes were observed in the nontapetal fundus, except vascular attenuation. The generalized funduscopic changes progressed, and especially the vascular attenuation became more marked ophthalmoscopically at age 10 months.

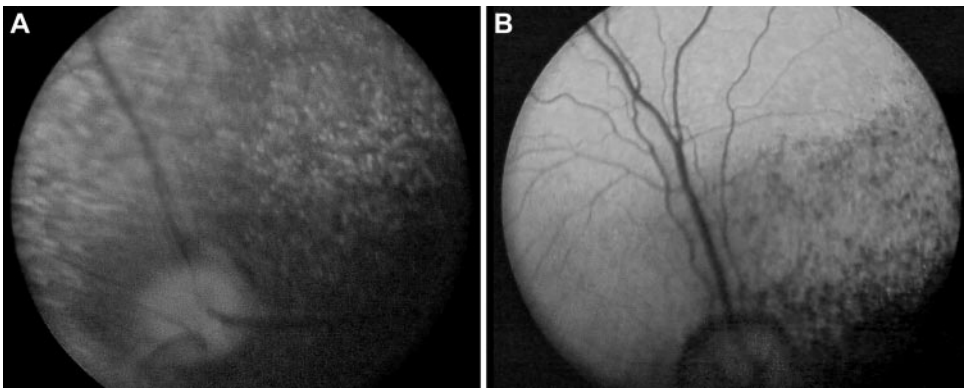

Figure 2. Fundus photographs obtained from the homozygous affected littermate, dog 1 (**A**) and from the homozygous normal littermate, dog 4 (**B**), at age 8 months, showing marked grayish discoloration and mottling in the tapetal fundus in the affected dog. Severe generalized vascular attenuation was also present.

Electroretinography

At 3 months of age, the ERG responses of the affected *TPP1*$^{-/-}$ dog (dog 1) did not differ significantly from the responses of the normal littermates under any of the stimulus conditions used (Fig. 3). The b-wave response amplitudes elicited by a low-intensity flash stimulus gradually increased over a 20-minute dark adaptation period in a similar manner in the affected and normal littermates. Scotopic flash stimuli at 3 and 10 cd-s/m^2 elicited a- and b-wave responses of similar amplitudes and implicit times in all the dogs at 3 months of age (Figs. 3, 4). Responses to both photopic single flash and flicker stimuli were similar in the affected *TPP1*$^{-/-}$ and in the littermates at this age (Fig. 3). By 7 months of age, however, the ERG responses in the affected dog were substantially altered, whereas no significant changes were observed in the other littermates (Figs. 3, 4). At 7 months, the b-waves elicited by a low-intensity flash stimulus were barely detectable at any time over a 20-minute period of dark adaptation in the affected dog (Fig. 3). At higher stimulus intensities under scotopic conditions, both a- and b-wave amplitudes were substantially decreased in the *TPP1*$^{-/-}$ dog compared with the responses elicited from the same dog at 3 months of age (Figs. 3, 4). The reductions in b-wave amplitudes were greater than those for a-wave amplitudes, resulting in a decrease in the b- to a-wave ratio (Table 1). Photopic response amplitudes also decreased in the affected dog between 3 and 7 months of age (Fig. 3).

These decreases in response amplitudes progressed through 10 months of age (Figs. 3, 4, 5), with a progressive decline in the b- to a-wave ratio in the scotopic flash ERG (Table 1). At 8 and 10 months of age, no b-wave was detectable in the affected dog at low stimulus intensity at any time during the dark adaptation period (Figs. 3, 5). The b-wave was replaced by an electronegative response. At higher stimulus intensities under scotopic conditions, an a-wave of increased implicit time was observed, and the b-wave did not reach baseline and had substantially increased noise levels relative to the littermates (Fig. 5). Under these conditions an electropositive spike was observed on the recording with an implicit time of ~70 ms. Photopic single flash stimulus did not elicit detectable a- or b-waves but did elicit a similar electropositive spike

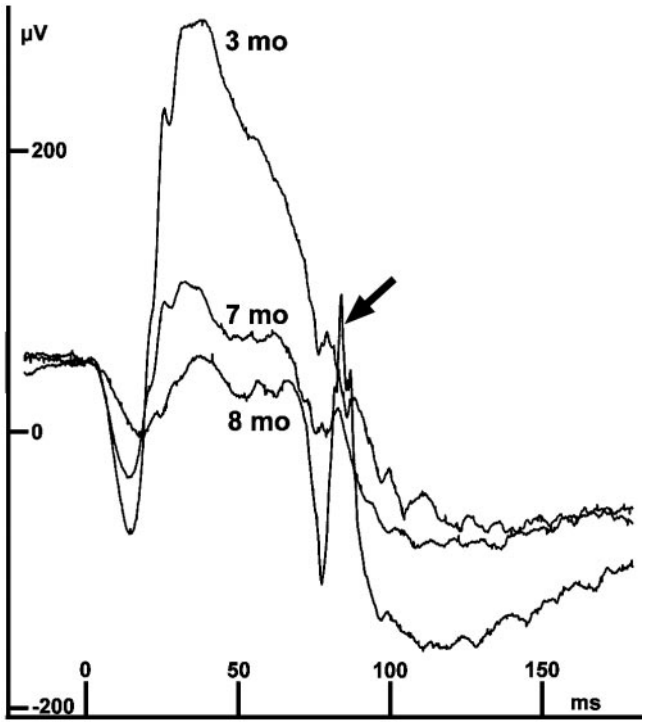

FIGURE 4. Comparison of ERG recordings using standard-intensity flash stimuli (3 cd-s/m^2) for the affected dog 1 at ages 3, 7, and 8 months. Note the successive reduction of a- and b-wave parameters, more so for the b-wave than for the a-wave with time. Also observe the longer implicit time of the a-wave and the high-amplitude spike in the recordings at age 8 months (*arrow*).

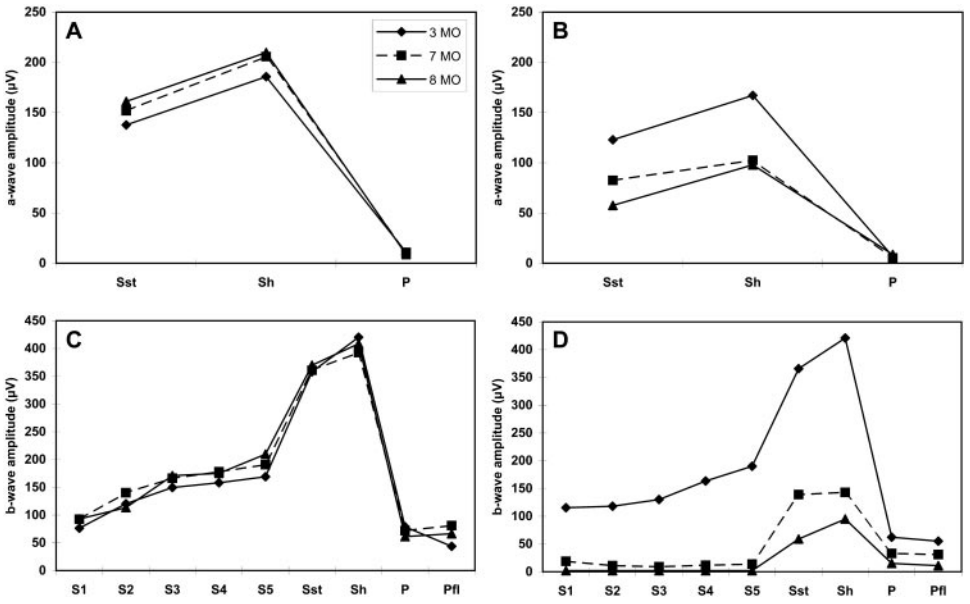

FIGURE 3. ERG a-wave (**A**, **B**) and b-wave (**C**, **D**) response amplitudes in a normal Dachshund (dog 4) (**A**, **C**) and in a littermate homozygous for the *TPP1* frameshift mutation (dog 1) (**B**, **D**). ERG data were obtained during recording sessions for scotopic low-intensity stimuli, 0.01 cd-s/m^2, during the process of dark adaptation (**C**, **D**; S1–S5), for scotopic standard flash (Sst, 3 cd-s/m^2) and scotopic high-intensity stimuli (Sh, 10 cd-s/m^2), and for photopic single flash (P) and 30-Hz flicker recordings (Pfl) (both at intensity 3 cd-s/m^2 after 10 minutes of light adaptation using a background of 30 cd/m^2).

TABLE 1. ERG b- to a-Wave Ratios in Response to 3 cd-s/m^2 Flashes in Scotopic Conditions

Dog	Dog Genotype	3 mo	7 mo	8 mo	10 mo
1	*TPP1*$^{-/-}$	2.9	1.6	1.0	0.6
2	*TPP1*$^{+/-}$	2.9	2.2	2.3	ND
3	*TPP1*$^{+/-}$	2.9	2.7	2.4	ND
4	*TPP1*$^{+/+}$	2.5	2.3	2.2	2.5

ND, not determined.

(Fig. 5). Flicker stimulation under photopic conditions elicited responses in the dog that were of much lower amplitudes and more irregular than those of the other littermates under the same conditions (Fig. 5). Positive electrical spikes were also observed on the ERG recordings for photopic flicker (Figs. 4, 5). The ERG responses of the unaffected dogs remained relatively unchanged throughout the observation period and the electropositive spikes were never observed in these animals.

Implicit times for b-waves in the *TPP1*$^{-/-}$ dog were comparable to those of the normal littermates at all ages examined. However, in the affected dog, the implicit time of the a-wave

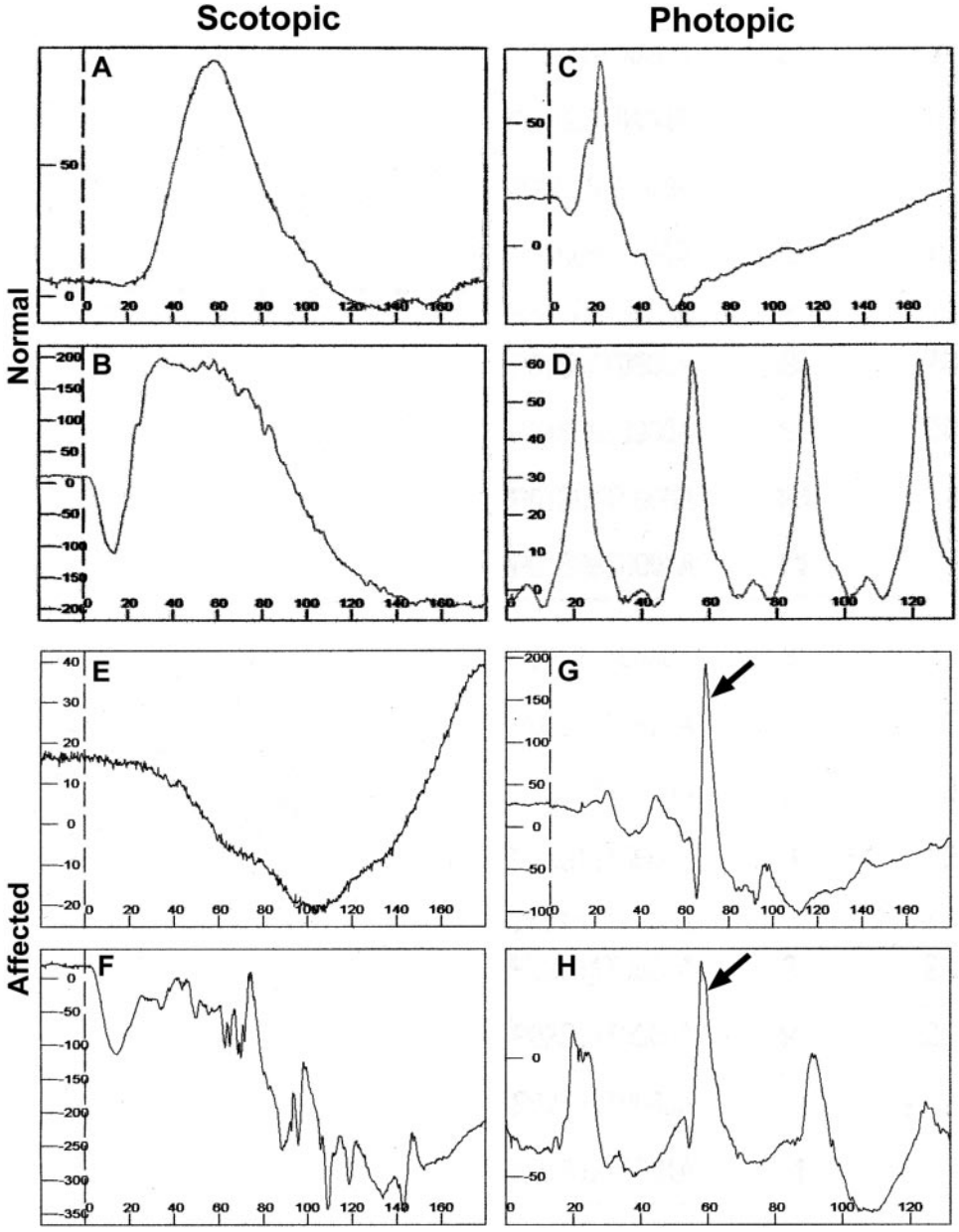

FIGURE 5. ERG responses of a normal Dachshund, dog 4 (**A**–**D**), and of a littermate homozygous for a frameshift mutation in the *TPP1* gene, dog 1 (**E**–**H**), at 10 months of age are shown: Responses obtained with a low-intensity flash stimulus (0.01 cd-s/m^2; **A**, **E**) and with a standard-intensity flash (3 cd-s/m^2; **B**, **F**) under scotopic conditions; responses obtained with single-flash stimulus under photopic conditions (5.1 Hz at 3 cd-s/m^2; **C**, **G**); responses to a 3 cd-s/m^2 flicker stimulus at 30 Hz under photopic conditions (**D**, **H**). Abnormal spikes in the photopic responses in the affected dog (*arrows*) may indicate light-induced seizure activity. The photopic recordings were performed after 10 minutes of light adaptation using 30 cd/m^2 of background light. For each recording, time in milliseconds (ms) is shown on the abscissa and amplitude in microvolts on the ordinate.

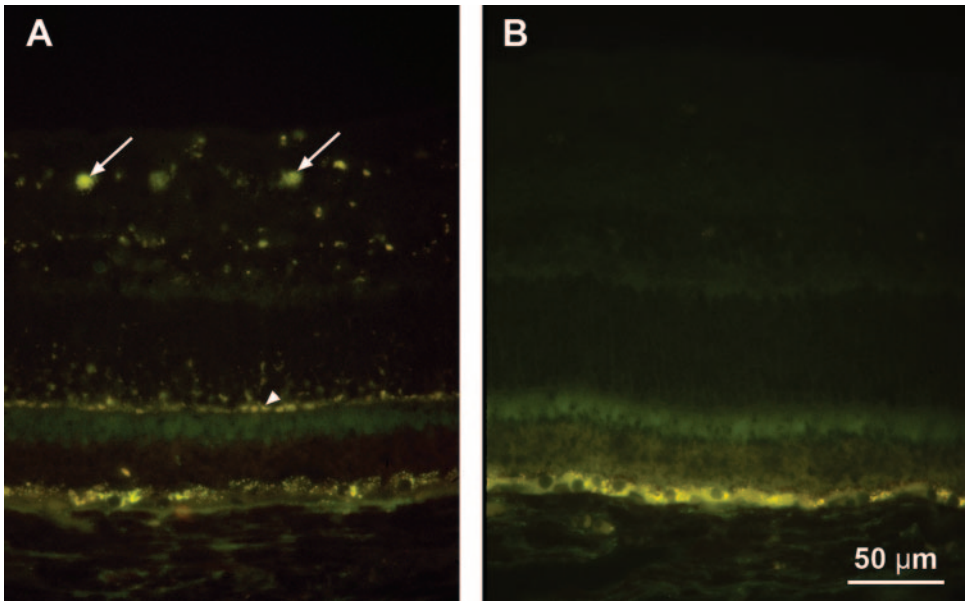

FIGURE 6. Fluorescence micrographs of unstained cryostat sections of the retinas from *TPP1*$^{-/-}$ (**A**) and *TPP1*$^{+/+}$ (**B**) littermate Dachshunds. Throughout the retina of the affected dog was *yellow*-emitting autofluorescent material that was particularly abundant in the ganglion cells (*arrows*) and along the outer limiting membrane (*arrowhead*). Inclusions with similar fluorescent properties were also present in the RPE of the *TPP1*$^{-/-}$ dog. In the retina of the *TPP1*$^{+/+}$ dog, *yellow*-emitting autofluorescent material was present only in the RPE.

elicited under scotopic conditions increased between 7 and 8 months of age (Fig. 4). This increase was maintained in the recordings at 10 months of age.

Morphologic Analyses

The dog that was homozygous for the *TPP1* frame-shift mutation exhibited autofluorescent storage material in most layers of the neural retina (Fig. 6A). The storage material was particularly abundant in ganglion cells and in a band just interior to the outer limiting membrane. Autofluorescent inclusions were also present in the RPE. There was no detectable autofluorescent material in the neural retinas of either the homozygous normal dog or the dog heterozygous for the *TPP1* mutation (Fig. 6B). Both of the latter dogs exhibited autofluorescent pigment in the RPE that appeared to be more abundant than in the RPE of the dog homozygous for the *TPP1* mutation.

Electron microscopic examination of the retina from the *TPP1*$^{-/-}$ dog indicated that the autofluorescent storage material consisted of membrane-bound cellular inclusions filled with a distinctive curvilinear substance (Fig. 7). The inclusions adjacent to the outer limiting membrane were localized to the photoreceptor cell bodies (Fig. 7B). No storage bodies containing the curvilinear substance were detected in the RPE.

The photoreceptor cell densities in the retina from the *TPP1*$^{-/-}$ dog were substantially lower than those in the retinas from the *TPP1*$^{+/+}$ and *TPP1*$^{+/-}$ littermates (Figs. 8, 9). In the superior region of the retina, the mean photoreceptor cell density in the *TPP1*$^{+/+}$ dog was 295 cells per 150 μm, whereas

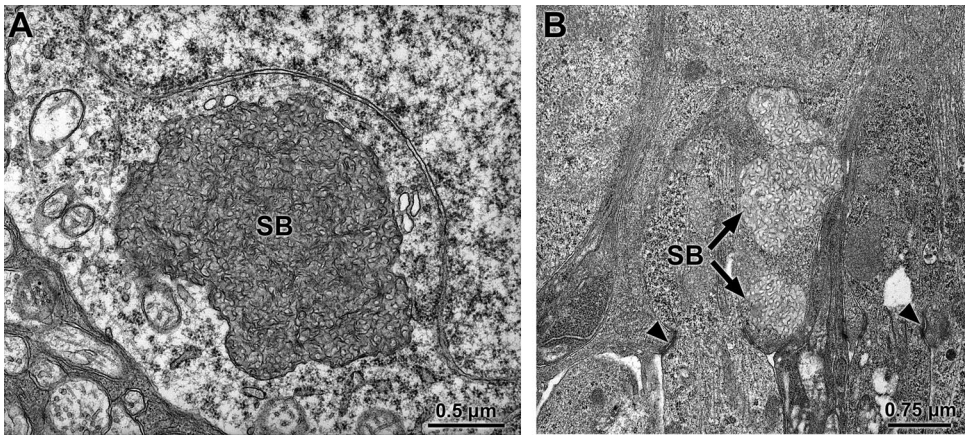

FIGURE 7. Electron micrographs showing the distinctive disease-specific storage bodies (SB) observed in the retinal ganglion cells (**A**) and photoreceptor cells (**B**) of the *TPP1*$^{-/-}$ dog. In the photoreceptor cells, the SBs were localized primarily just interior to the outer limiting membrane (*arrows*). Cell junctional complexes that make up the outer limiting membrane are indicated by *arrowheads* in (**B**). The micrograph in (**B**) is oriented such that the inner retina is toward the top.

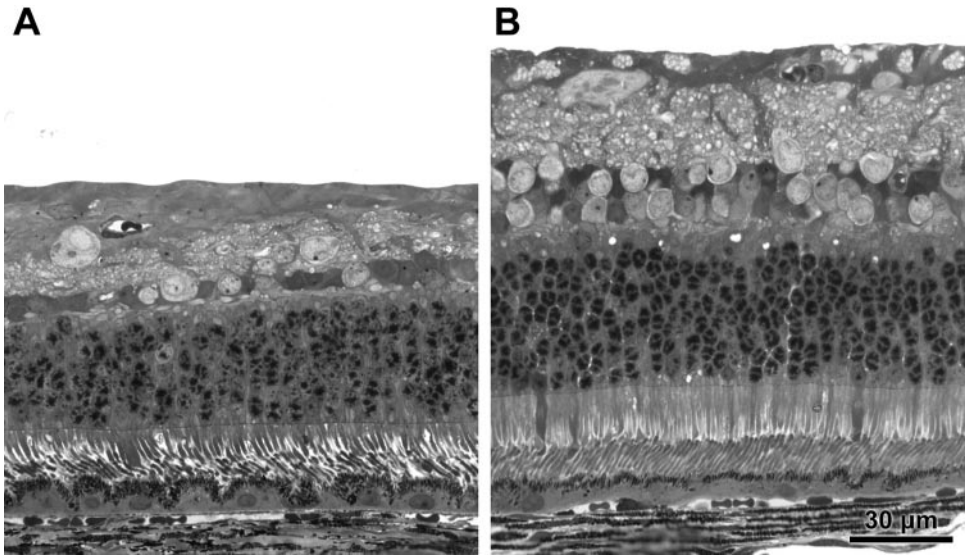

FIGURE 8. Light micrographs of the inferior–central retinas of *TPP1*$^{-/-}$ (**A**) and *TPP1*$^{+/+}$ (**B**) littermate Dachshunds. The overall thickness of the retina was much less in the *TPP1*$^{-/-}$ dog, there were far fewer nuclei in the inner nuclear layer, and the photoreceptor outer segments were less dense and less regularly organized.

in the *TPP1*$^{-/-}$ dog, it was only 203 cells per 150 μm. In the heterozygous dog, the mean photoreceptor cell density in this region was 297 cells per 150 μm. In the inferior region of the retina, the mean photoreceptor cell density in the *TPP1*$^{+/+}$ dog was 224 cells per 150 μm but in the *TPP1*$^{-/-}$ dog, it was only 150 cells per 150 μm. In the heterozygous dog, the mean photoreceptor cell density in this region was 193 cells per 150 μm.

The cell density in the inner nuclear layer was also lower in the *TPP1*$^{-/-}$ dog than in either the *TPP1*$^{+/+}$ or *TPP1*$^{+/-}$ littermates (Figs. 8, 9). In the superior region of the retina, there was a mean of 72 nuclei per 150 μm in the INL of the *TPP1*$^{+/+}$ dog and only 30 in the *TPP1*$^{-/-}$ animal. In the *TPP1*$^{+/-}$ dog, the INL cell density in the inferior retina was 72 cells per 150 μm. In the inferior region of the retina, there was a mean of 67 nuclei per 150 μm in the INL of the *TPP1*$^{+/+}$ dog and only 31 in the *TPP1*$^{-/-}$ animal. In the *TPP1*$^{+/-}$ dog, the INL cell density in the inferior retina was 51 cells per 150 μm.

The photoreceptor outer segments in the *TPP1*$^{-/-}$ dog were much more irregular in shape and size than those in the *TPP1*$^{+/+}$ or *TPP1*$^{+/-}$ littermate retinas (Figs. 8, 10). There was also substantially more intercellular space in the inner and outer segment regions in the *TPP1*$^{-/-}$ dog than in the unaffected littermates (Figs. 8, 10). In the affected dog, most of the RPE cells were mounded in the center, whereas RPE cells in the unaffected dogs were relatively uniform in height (Fig. 8).

DISCUSSION

Blindness is one of the hallmarks of the neuronal ceroid lipofuscinoses, including the late infantile form. Children with late infantile NCL have apparently normal vision at birth, but experience progressive vision loss in early childhood that culminates in total blindness. ERG analyses of affected children younger than 5 years demonstrated profoundly subnormal b-wave amplitudes under both scotopic and photopic conditions, whereas a-wave amplitudes were less severely affected.[26] These abnormalities were very similar to those observed in the dog with the *TPP1* mutation, and indicate that the inner retina is affected first in this disease. Photoreceptor cell degeneration eventually occurs in the human disorder, as indicated by morphologic studies of eyes obtained after death.[27–29] At the end stage of the disease in humans, photoreceptor cell degeneration and loss is as profound as the degeneration of the inner nuclear layer. Through intensive care, children who have late infantile NCL are able to survive long after they become blind and severely impaired neurologically. Thus, morphologic data do not exist to indicate the structural integrity of the retina at stages of the disease when retinal responses to light stimuli can still be recorded. However, the similarities of the ERG changes observed in the dog with the *TPP1* mutation to those observed in the early disease stages in children suggests that cell loss in the inner retina proceeds more rapidly than photoreceptor cell loss in the human disease, as it does in the dog model. Degenerative changes in the photoreceptors were observed in the affected dog at 10.5 months of age, and these changes may have progressed further had the dog been kept alive longer.

The peak of the a-wave in the scotopic ERG elicited at 3 cd-s/m^2 in the affected dog is delayed starting at 8 months of age (Fig. 4). The negative onset of the a-wave reflects the start of the response generated by the photoreceptor cells,[30] and the positive-going portion corresponds to onset of the response of the inner retina (mainly bipolar cell activity). Therefore, the timing of the a-wave peak depends on the balance between the photoreceptor and inner retinal responses. The delay in the peak of the a-wave seen at later stages of the disease in the affected dog may represent alterations in the kinetics of the responses of the photoreceptor cells, the inner retina or both. The fact that the inner retina is more profoundly affected in this disease suggests that the delay results primarily from alterations in function of the bipolar cells.

The affected dog was functionally blind by the age of 8 months at a time when ERG responses could still be elicited with sufficiently intense stimuli. Even in a brightly lit room, the dog did not blink or otherwise respond to rapid hand movements toward its face, nor did it follow objects with its gaze. Changes in spontaneous behavior also indicated that the dog was blind by 8 months of age. This suggests that central nervous system changes may contribute significantly to the loss of vision in the disease. Consistent with this conclusion was our observation that decreases in the visual evoked potential preceded the ERG changes in the affected dog (data not

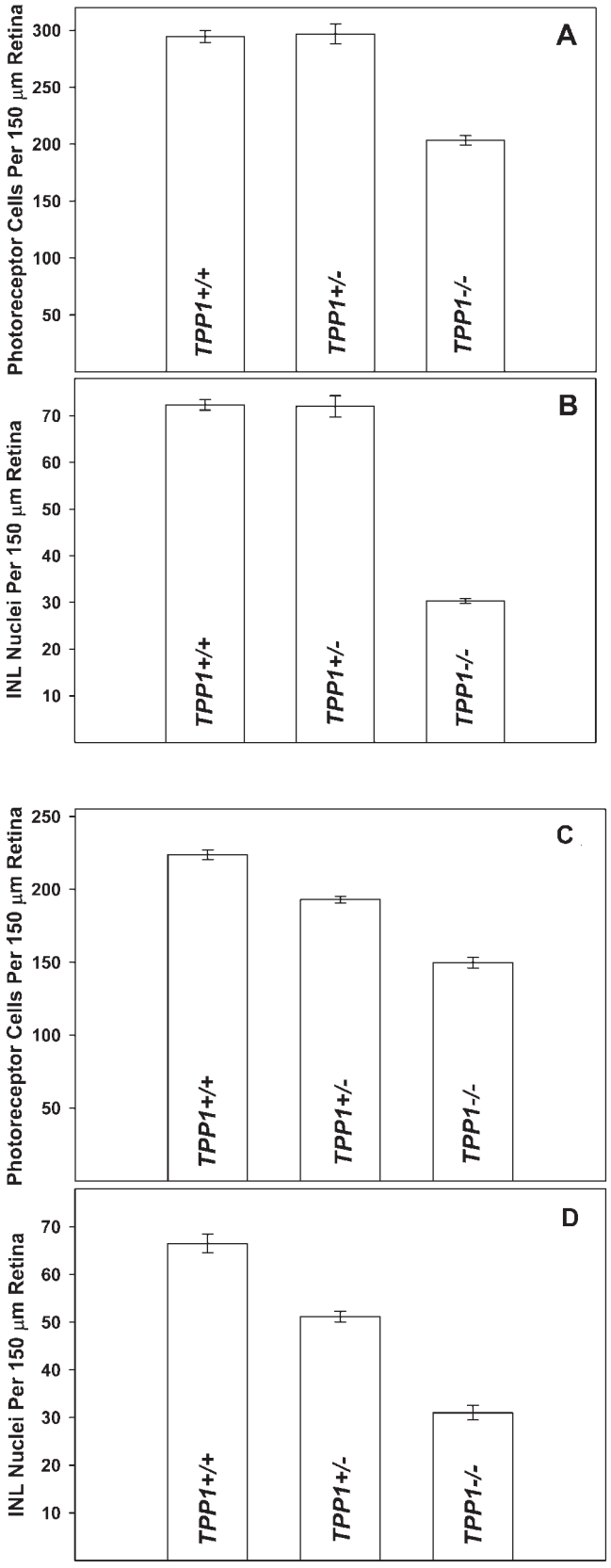

FIGURE 9. Cell densities in the (**A**) outer nuclear (photoreceptors) and (**B**) inner nuclear layers from the superior retinas of $TPP1^{+/+}$, $TPP1^{+/-}$, and $TPP1^{-/-}$ littermate Dachshunds. Cell densities in the (**C**) outer nuclear (photoreceptors) and (**D**) inner nuclear layers from the inferior retinas of $TPP1^{+/+}$, $TPP1^{+/-}$, and $TPP1^{-/-}$ littermate Dachshunds. Bars indicate means and standard errors of at least six determinations in each eye.

shown). It is possible that degeneration of the optic nerve contributed to the loss of vision while ERG responses could still be elicited. Indeed, optic nerve degeneration has been reported in mouse models of the NCLs.[15,31,32]

In the affected Dachshund, disease-specific storage body accumulation was observed in ganglion cells, cells of the inner nuclear layer, and in the photoreceptor cells at 10.5 months of age (Figs. 6, 7). In human subjects who died as a result of advanced late infantile NCL, storage body accumulation was observed not only in these retinal layers, but also in many other cell types in the retina, including the retinal pigment epithelium (RPE) and macrophages that had invaded the retina.[27] These observations indicate that the retinal degeneration becomes much more profound if affected individuals can be kept alive long enough. The presence of disease-specific storage material in the RPE in late-stage human late infantile NCL was reported based on electron microscopic analyses.[28] Fluorescence microscopy cannot be used reliably to assess storage material accumulation in the RPE because lipofuscin, with nearly identical fluorescence properties, accumulates in the RPE as a part of the normal aging process (Fig. 6).[33–35] However, the ultrastructural appearance of the storage material that accumulates in late infantile NCL is quite distinctive from that of RPE lipofuscin. We did not observe any accumulation of this storage material in the RPE of the affected dog with electron microscopy, which suggests that the accumulation of this material in the RPE of human patients may occur late in the disease. With fluorescence microscopy, it appeared that the affected dog actually had less autofluorescent pigment in the RPE than did its unaffected littermates (Fig. 6). It has been shown that RPE lipofuscin accumulation is dependent on the presence and function of the photoreceptor cells,[36–42] so this apparent reduced lipofuscin accumulation may reflect the loss and abnormal function of photoreceptor cells.

Despite some loss of photoreceptor cells at the time the affected dog was euthanatized, clearly the RPE was still active in outer segment phagocytosis and degradation via the lysosomal pathway. Therefore, it was somewhat surprising that the RPE did not exhibit an accumulation of the disease-related inclusions. The normal substrates for TPP1 are not known. Perhaps the lack of storage body accumulation in the RPE indicates that the material normally degraded by TPP1 is not present in the phagocytosed material. Substrate specificity would explain why storage material is more pronounced in some cell types than in others. The RPE may also have mechanisms for disposing of the normal substrates of TPP1 that other cells, such as inner retinal neurons, do not. Among the other NCLs, some exhibit RPE storage body accumulation while others do not.[2,21,27,29,43–46]

It is not known whether storage body accumulation in the NCLs is itself detrimental. However, this accumulation certainly correlates with pathology at the cellular level. Thus, although retinal ganglion cell function is not assessed with the ERG, the accumulation of storage material in these cells suggests that they may be functionally impaired. Abnormalities in ganglion cell function may at least partially account for the fact that functional blindness and alterations in the pupillary light reflex precede complete loss of retinal responses to light as assessed by the ERG.

Overall, it appears that the $TPP1^{-/-}$ dog is an excellent model for the ocular features of late infantile NCL. In both affected humans and dogs, the retina develops normally, but then undergoes progressive degeneration as the disease progresses. Funduscopic changes are similar in the human and canine diseases,[26] as are changes in vision, retinal function, and morphology.

The TPP1 protein is a soluble lysosomal enzyme that can be exchanged between cells and that can therefore be supplied

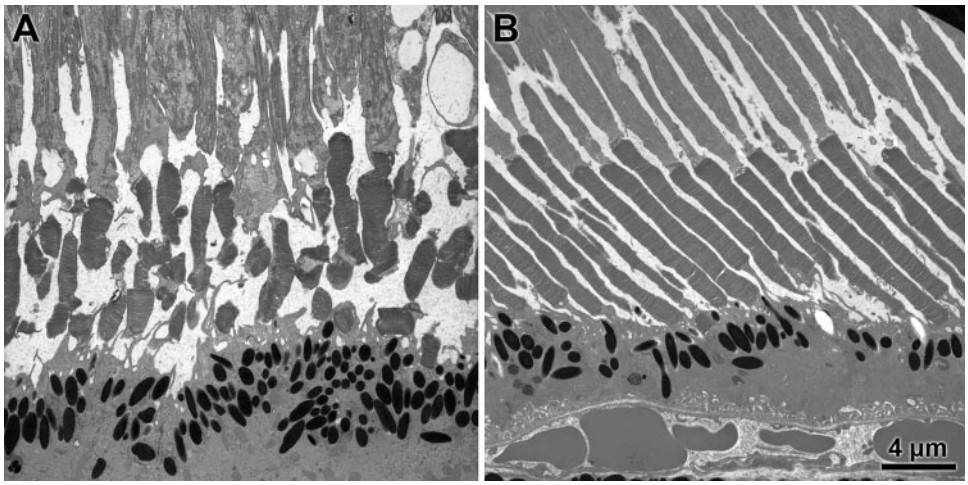

FIGURE 10. Electron micrographs of the outer retinas from the inferior-central retinas of $TPP1^{-/-}$ (**A**) and $TPP1^{+/+}$ (**B**) dogs. The photoreceptor outer segments in the $TPP1^{-/-}$ dog are much less regular in morphology and orientation, as well as being less densely packed.

exogenously to deficient cells.[47,48] Based on this fact, studies are being conducted to determine the potential efficacy of gene and stem cell therapies for treating this disorder.[13,49] The dog provides an excellent model in which to evaluate these therapies, particularly with respect to rescuing the retina. Profound deficiencies in retinal function develop relatively slowly in humans and in the canine model, and so there is a fairly large time window during which therapeutic intervention could prevent degenerative changes. The morphologic data indicate that late in the disease cell loss from the retina is substantial, so late therapeutic interventions are unlikely to be effective in restoring vision.

Acknowledgments

The authors thank Cheryl Jensen, Melainia McClain, and Randy Tindall of the University of Missouri Electron Microscopy Core Facility for expert assistance and Leilani Castaner for superb animal care.

References

1. Wisniewski K, Zhong N, eds. *Batten Disease: Diagnosis, Treatment, and Research*. New York: Academic Press; 2001.
2. Bensaoula T, Shibuya H, Katz ML, et al. Histopathologic and immunocytochemical analysis of the retina and ocular tissues in Batten disease. *Ophthalmology*. 2000;107:1746–1753.
3. Wisniewski KE, Kida E, Golabek AA, et al. Neuronal ceroid lipofuscinoses: classification and diagnosis. In: Wisniewski KE, Zhong N, eds. *Batten Disease: Diagnosis, Treatment, and Research*. New York: Academic Press; 2001.
4. Dyken PR. Reconsideration of the classification of the neuronal ceroid-lipofuscinoses. *Am J Med Genet Suppl*. 1988;5:69–84.
5. Goebel HH, Wisniewski KE. Current state of clinical and morphological features in human NCL. *Brain Pathol*. 2004;14:61–69.
6. Siintola E, Partanen S, Stromme P, et al. Cathepsin D deficiency underlies congenital human neuronal ceroid-lipofuscinosis. *Brain*. 2006;129:1438–1445.
7. Siintola E, Topcu M, Aula N, et al. The novel neuronal ceroid lipofuscinosis gene MFSD8 encodes a putative lysosomal transporter. *Am J Hum Genet*. 2007;81:136–146.
8. Steinfeld R, Reinhardt K, Schreiber K, et al. Cathepsin D deficiency is associated with a human neurodegenerative disorder. *Am J Hum Genet*. 2006;78:988–998.
9. Birch DG. Retinal degeneration in retinitis pigmentosa and neuronal ceroid lipofuscinosis: an overview. *Mol Genet Metab*. 1999;66:356–366.
10. Eksandh L, Ponjavic V, Munroe P, et al. Full-field ERG in patients with Batten/Spielmeyer-Vogt disease caused by mutations in the CLN3 gene. *Ophthalmic Genet*. 2000;21:69–77.
11. Horiguchi M, Miyake Y. Batten disease; deteriorating course of ocular findings. *Jpn J Ophthalmol*. 1992;36:91–96.
12. Weleber RG, Gupta N, Trzupek KM, et al. Electroretinographic and clinicopathologic correlations of retinal dysfunction in infantile ceroid lipofuscinosis (infantile Batten disease). *Mol Genet Metab*. 2004;83:128–137.
13. Crystal RG, Sondhi D, Hackett NR, et al. Clinical protocol: administration of a replication-deficient adeno-associated virus gene transfer vector expressing the human CLN2 cDNA to the brain of children with late infantile neuronal ceroid lipofuscinosis. *Hum Gene Ther*. 2004;15:1131–1154.
14. Steiner R, Koch T, Al-Uzri A, et al. A phase 1 clinical study of human CNS stem cells (HuCNS-SC) in patients with neuronal ceroid lipofuscinosis. In: Pearce D, Jalanki A, eds. *11th International Congress on Neuronal Ceroid Lipofuscinosis*. Rochester, NY; 2007.
15. Katz ML, Johnson GS, Tullis GE, Lei B. Phenotypic characterization of a mouse model of juvenile neuronal ceroid lipofuscinosis. *Neurobiol Dis*. 2007;29:242–253.
16. Jolly RD. Comparative biology of the neuronal ceroid-lipofuscinoses (NCL): an overview. *Am J Med Genet*. 1995;57:307–311.
17. Jolly RD, Palmer DN, Studdert VP, et al. Canine ceroid-lipofuscinosis: a review and classification. *J Small Anim Pract*. 1994;35:299–306.
18. Jolly RD, Martinus RD, Palmer DN. Sheep and other animals with ceroid-lipofuscinosis: their relevance to Batten disease. *Am J Med Genet*. 1992;42:609–614.
19. Katz ML, Shibuya H, Johnson GS. Animal models for the ceroid lipofuscinoses. *Adv Genet*. 2001;45:183–203.
20. Katz ML, Johnson GS, Drögemüller C. Canine neuronal ceroid lipofuscinoses. In: Mole SE, Lake BD, Goebel HH, eds. *The Neuronal Ceroid Lipofuscinoses* (*Batten Disease*). 2nd ed. London: IOS Press; in press.
21. Narfstrom K, Wrigstad A, Ekesten B, Berg AL. Neuronal ceroid lipofuscinosis: clinical and morphologic findings in nine affected Polish Owczarek Nizinny (PON) dogs. *Vet Ophthalmol*. 2007;10:111–120.
22. Awano T, Katz ML, Sohar I, et al. A frame shift mutation in the canine ortholog of human *CLN2* in a juvenile dachshund with neuronal ceroid lipofuscinosis. *Mol Genet Metab*. 2006;89:254–260.
23. Lorenz MD, Kornegay JN. Neurologic history and examination. In: Lorenz MD, Kornegay JN, eds. *Handbook of Veterinary Neurology*. 4th ed. St. Louis: Saunders-Elsevier Science; 2004:3–46.

24. Narfstrom K, Ekesten B, Rosolen SG, et al. Guidelines for clinical electroretinography in the dog. *Doc Ophthalmol*. 2002;105:83–92.
25. Marmor MF, Holder GE, Seeliger MW, Yamamoto S. Standard for clinical electroretinography (2004 update). *Doc Ophthalmol*. 2004;108:107–114.
26. Weleber RG. The dystrophic retina in multisystem disorders: the electroretinogram in neuronal ceroid lipofuscinoses. *Eye*. 1998;12:580–590.
27. Traboulsi EI, Green WR, Luckenbach MW, de la Cruz ZC. Neuronal ceroid lipofuscinosis: ocular histopathologic and electron microscopic studies in the late infantile, juvenile and adult forms. *Graefes Arch Clin Exp Ophthalmol*. 1987;225:391–402.
28. Goebel HH, Zeman W, Damaske E. An ultrastructural study of the retina in the Jansky-Bielchowsky type of neuronal ceroid lipofuscinosis. *Am J Ophthalmol*. 1977;83:70–79.
29. Schochet SS, Font RL, Morris HH. Jansky-Bielschowsky form of neuronal ceroid lipofuscinosis: ocular pathology of the Batten-Vogt syndrome. *Arch Ophthalmol*. 1980;98:1083–1088.
30. Frishman LJ, Steinberg RH. Origin of negative potentials in the light-adapted ERG of cat retina. *J Neurophysiol*. 1990;63:1333–1346.
31. Sappington RM, Pearce DA, Calkins DJ. Optic nerve degeneration in a murine model of juvenile ceroid lipofuscinosis. *Invest Ophthalmol Vis Sci*. 2003;44(9):3725–3731.
32. Weimer JM, Custer AW, Benedict JW, et al. Visual deficits in a mouse model of Batten disease are the result of optic nerve degeneration and loss of dorsal lateral geniculate thalamic neurons. *Neurobiol Dis*. 2006;22:284–293.
33. Feeney L. Lipofuscin and melanin of human retinal pigment epithelium: fluorescence, enzyme cytochemical, and ultrastructural studies. *Invest Ophthalmol Vis Sci*. 1978;17:583–600.
34. Katz ML, Robison WG. Age-related changes in the retinal pigment epithelium of pigmented rats. *Exp Eye Res*. 1984;38:137–151.
35. Wing GL, Blanchard GC, Weiter JJ. The topography and age relationship of lipofuscin concentration in the retinal pigment epithelium. *Invest Ophthalmol Vis Sci*. 1978;17:601–607.
36. Katz ML, Drea CM, Robison WG. Relationship between dietary retinol and lipofuscin in the retinal pigment epithelium. *Mech Age Dev*. 1986;35:291–305.
37. Katz ML, Drea CM, Eldred GE, et al. Influence of early photoreceptor degeneration on lipofuscin in the retinal pigment epithelium. *Exp Eye Res*. 1986;43:561–573.
38. Katz ML, Eldred GE, Robison WG. Lipofuscin autofluorescence: evidence for vitamin A involvement in the retina. *Mech Age Dev*. 1987;39:81–90.
39. Katz ML, Robison WG, Drea CM. Factors influencing lipofuscin accumulation in the retinal pigment epithelium. In: Totaro EA, Glees P, Pisanti FA, eds. *Advances in Age Pigments Research*. Oxford, UK: Pergamon Press; 1987:111–131.
40. Katz ML, Eldred GE. Retinal light damage reduces autofluorescent pigment deposition in the retinal pigment epithelium. *Invest Ophthalmol Vis Sci*. 1989;30:37–43.
41. Katz ML, Shanker MJ. Development of lipofuscin-like fluorescence in the retinal pigment epithelium in response to protease inhibitor treatment. *Mech Age Dev*. 1989;49:23–40.
42. Katz ML. Incomplete proteolysis may contribute to lipofuscin accumulation in the retinal pigment epithelium. *Adv Exp Med Biol*. 1990;266:109–118.
43. Goebel HH, Kohnene B, Koppang N, Armstrong D. Ultrastructural studies on the retinal pigment epithelium in the neuronal ceroid-lipofuscinoses. *Ophthalmic Paediatr Genet*. 1983;3:29–37.
44. Zeman W. Batten disease: ocular features, differential diagnosis and diagnosis by enzyme analysis. *Birth Defects*. 1976;12:441–453.
45. Goebel HH, Fix JD, Zeman W. The fine structure of the retina in neuronal ceroid-lipofuscinosis. *Am J Ophthalmol*. 1974;77:25–39.
46. Goebel HH. Neuronal ceroid-lipofuscinoses: the current status. *Brain Dev*. 1992;14:203–211.
47. Lin L, Lobel P. Production and characterization of recombinant human CLN2 protein for enzyme-replacement therapy in late infantile neuronal ceroid lipofuscinosis. *Biochem J*. 2001;357:49–55.
48. Sohar I, Sleat DE, Jadot M, Lobel P. Biochemical characterization of a lysosomal protease deficient in classical late infantile neuronal ceroid lipofuscinosis (LINCL) and development of an enzyme-based assay for diagnosis and exclusion of LINCL in human specimens and animal models. *J Neurochem*. 1999;73:700–711.
49. Stem Cells, Inc. announces an important milestone in Batten disease clinical trial (news release). *The Illuminator*. 2007;19:1.